Estimating soil available water capacity within a Mediterranean vineyard watershed using satellite imagery and crop model inversion

Mohamed Alkassem-Alosman, Samuel Buis, Guillaume Coulouma, Frédéric Jacob, Philippe Lagacherie, Laurent Prevot

Estimating soil available water capacity within a Mediterranean vineyard watershed using satellite imagery and crop model inversion

Mohamed Alkassem [a], Samuel Buis [b], Guillaume Coulouma [a], Frédéric Jacob [c], Philippe Lagacherie [a*], Laurent Prévot [a]

a. INRAE / UMR LISAH, University of Montpellier, INRAE, IRD, Institut Agro Montpellier, Montpellier, France
b. INRAE / UMR EMMAH, University of Avignon, INRAE, Avignon, France
c. IRD / UMR LISAH, University of Montpellier, INRAE, IRD, Institut Agro Montpellier, Montpellier, France

* Corresponding author:

- INRAE, UMR LISAH, 2 Place Viala 34060, Montpellier, Cedex 1, France.
- E-mail address: philippe.lagacherie@inrae.fr

Abstract

Soil available water capacity (SAWC) is a key factor to be considered when assessing soil capability to provide ecosystem services. The current study deepens the use of remotely sensed data for mapping SAWC and its components from crop model inversion. The inversion was conducted using the STICS (Simulateur mulTIdiscplinaire pour les Cultures Standard) crop model along with the GLUE (Generalized Likelihood Uncertainty Estimation) algorithm on a panel of 14 sites within a rainfed vineyard catchment located in Southern France. Several constraint variables derived from Landsat 7 ETM+ satellite imagery (leaf area index - LAI - and evapotranspiration - ET) or in-situ measurements (surface soil moisture - SSM), were used in the inversion process alone or in combination.

Three main outcomes could be reported when comparing retrievals of both SAWC and its components against field estimates. First, retrievals were significantly correlated with ground estimates for some SAWC components and some scenarios of constraint variables, although overall retrieving performances were quite poor. Second, poor retrieving performances for two scenarios of constraint variables were related to few sites for which specific processes were disregarded by the modelling framework, namely allochthonous water supply and waterlogging during wet autumn and summer. Third, we could identify some promising combinations of constraint variables, after the removal of the aforementioned sites with specific processes. These promising combinations were (LAI, ET) and even more (LAI, ET, SSM) for estimating SAWC and root zone thickness, as well as SSM for estimating soil moistures at field capacity and wilting point of the topsoil layer. Provided we can avoid site-specific processes, our approach may further provide spatial sampling of SAWC and related components, to be used as surrogate input data for DSM models.

Keywords: Digital Soil Mapping, remote sensing, crop model, inverse modelling, vineyard, soil available water capacity

1. Introduction

Soil Available Water Capacity (SAWC) is defined as the maximum amount of plant available water a soil can provide (USDA-NCRS, 2008). It is a well-known concept that has been used for long to express the capacity of soils to store water for plants (Veihmayer and Hendrickson, 1927). SAWC has also been used for characterizing important soil functions such as biomass production, erosion and flood control, water regulation and purification (Adhikari & Hartemink, 2016). SAWC is therefore a key factor to be considered when assessing soil capability to provide ecosystem services (McBratney et al., 2014). SAWC maps are thus required for applications based on soil capability over large territories (Leenaars et al., 2018).

SAWC mapping is often hampered by low number of sites on which SAWC values can be determined, since SAWC determination requires costly and time-consuming soil observations and soil property measurements. The most current technique for SAWC mapping consists of using conventional soil maps that require few SAWC measurements only at representative sites of different soil classes (e.g., Dejong and Shields, 1988). However, Leenhardt et al. (1994) showed that this approach had strong limitations in spatial resolution and accuracy, because the scale of conventional soil maps is often less than 1:25,000. More recently, several attempts were made to apply the principle of Digital Soil Mapping (DSM) for SAWC mapping (Piedallu et al., 2011, Leennars et al., 2018, Roman Dobarco et al., 2019, Styc & Lagacherie, 2021).

The general principle of DSM is to predict soil properties by machine learning and/or geostatistical models (McBratney et al., 2003). Both methods use available spatial data related to soil forming factors (e.g., relief, climate, geology), and they are calibrated over in-situ measurements of soil properties across several sites. In the case of SAWC that is characterized by scarcity of in-situ measurements, pedotransfer functions (PTF) have been used to estimate SAWC components from easy-to-measure soil properties (Van Looy, 2017). However, validation ex-

ercises showed that the mapping performances remained low as compared to other soil properties, with a non-negligible PTF contribution to the overall uncertainty (Roman Dobarco et al., 2019). Therefore, increasing the number of in-situ SAWC estimates is a pre-requisite for improving SAWC maps produced by DSM approaches.

Remote sensing represents a valuable source of proxy that may deliver spatial estimates of several surface soil properties, with fine spatial resolutions and over vast spatial extents, but they cannot be considered as possible techniques for a direct determination of SAWC. As far as soil properties are concerned, some of them (e.g., clay, organic carbon, calcium carbonate) have been successfully predicted from Vis-NIR hyperspectral remote sensing (Gomez et al., 2012), Vis-NIR multispectral remote sensing (Vaudour et al., 2019) or gamma-ray spectroscopy (Wilford, 2006). Recent studies reported some promising capabilities with reflectance or emissivity spectra over the thermal infrared domain ([8 - 14] µm), but this remains prospective (Eisele et al., 2015). Besides, such remote sensing methods are restricted to the retrieval of topsoil properties, since deeper soil layers remain inaccessible.

A possible alternative to overcome this problem consists of using remotely sensed proxies of the soil-plant system characteristics, to be combined with dynamic models that simulate plant growth in relation to SAWC. Although some prospective studies can be found in the DSM literature (Taylor et al., 2013, Jin et al., 2018a), this alternative has been much more investigated in the remote sensing community, through the use of inverse modelling. Inverse modelling is the process of calculating, from a set of observations, the causal factors that produced them (Knighton et al., 2019). It can be applied to SAWC mapping by assuming that SAWC is the predominant causal factor of soil / plant variables observed from remote sensors, from which SAWC can therefore be retrieved. Within this framework, estimates of SAWC, or of its components, are obtained by using optimization techniques (Lammoglia et al., 2019; Prévot et al., 2003) or Bayesian methods (Mertens et al., 2004; Scharnagl et al., 2011). These approaches

iteratively reduce the differences between remotely sensed observations of soil / plant variables and simulations from crop / Soil Vegetation Atmosphere Transfer (SVAT) model, by modulating model values of SAWC or of its components.

Several soil and crop variables accessible from remote sensors have been considered as constraint variables for estimating SAWC components, following inverse modelling approaches. On the basis of mechanistic soil water models combined with soil evaporation and plant transpiration, several studies explored the retrieval of soil depth and hydraulic properties, (1) from topsoil moisture (Montzka et al., 2011), (2) from both topsoil and root zone soil moistures (Galleguillos et al., 2011a; b; 2017), (3) from surface temperature in relation to root zone soil moisture (Coudert et al., 2006; Guillevic et al., 2012; Dong et al., 2016), (4) from both surface soil moisture and surface temperature (Ridler et al., 2012), or (5) from evapotranspiration (Olioso et al., 2002). Other studies relied on crop models (1) with plant canopy variables such as leaf area index (LAI) or nitrogen absorption (Ferrant et al., 2016; Guerif et al., 2006; Launay et al., 2005; Varella et al., 2010a), (2) with both LAI and surface soil moisture (Dente, 2008; Sreelash et al., 2017), or (3) with both LAI and evapotranspiration (Charoenhirunyingyos et al., 2011).

The panel of studies above-discussed have provided valuable insights about the opportunities offered by the joint use of mechanistic models and remotely sensed observations. Nevertheless, several methodological developments still are necessary for improving performances of SAWC retrieving. First, the use of LAI as constraint variable has been extensively addressed, whereas the use of surface temperature and evapotranspiration, both related to root zone soil moisture, was moderately investigated (Feddes et al., 1993; Jhorar et al., 2004; Singh et al., 2010), because of methodological challenges related to the turbulent nature of surface temperature and surface heat fluxes (Lagouarde et al., 2013). However, including surface temperature and evapotranspiration into the panel of constraint variables is likely to improve the performances of

SAWC retrieving from model inversion, and even more when considering operational satellite that provide observations on a routine basis. Second, most studies focused on quite homogeneous vegetation canopies, and few of them only investigated heterogenous or discontinuous canopies, whereas the structural properties of such canopies induce methodological challenges in relation to the partitioning of energy fluxes (Kool et al., 2014; Montes et al., 2014). Third, most studies focusing on SAWC retrieving were conducted at the field scale, by involving heavy experiments with numerous field measurements of soil and crop variables, whereas very few studies investigated the regional extent (Todoroff et al., 2010; Coops et al., 2012). This is all the more critical that the regional extent is appropriate for DSM while inducing methodological challenges related to landscape heterogeneities (e.g., climate, soil, crops), whereas no validation against SAWC ground-based measurements has been reported to date.

The current study aimed to estimate SAWC and its components from crop model inversion. The SAWC components to be estimated were root zone thickness as well as soil moistures at field capacity and wilting point for topsoil and root zone layers. Crop model inversion relied on three constraint variables, to be used alone or in combination, namely leaf area index (LAI) and actual evapotranspiration (ET), both obtained from satellite remotely sensed data, and surface soil moisture (SSM) derived from in-situ measurements, because remote sensing of SSM remains questionable over vineyards (Lei et al., 2020). The experiment was conducted on a panel of 14 sites within a heterogeneous landscape with discontinuous vegetation canopies, namely a rainfed vineyard catchment located in Southern France. In order to address landscape scale heterogeneity, we used remotely sensed observations with high spatial resolution only, namely Landsat 7 ETM+ data that are operationally collected. The inversion modelling was conducted using the crop model STICS (Simulateur mulTIdiscplinaire pour les Cultures Standard, Brisson et al., 1998) along with the GLUE inversion algorithm (Generalized Likelihood Uncertainty Estimation, Beven et al., 1992). These methodological tools were chosen for their

138 robustness with regards to former studies at the field scale (Jin et al., 2018b). The paper is
139 structured as following. We first present the methodological strategy, including the experi-
140 mental setup, the data set with variability in SAWC ground-based measurements, and crop
141 model inversion. We next present the inversion results, including the capability of the inversion
142 procedure to make agreement between observations and crop model simulations, and the relia-
143 bility of SAWC estimates from the inversion procedure. We finally discuss these results in
144 terms of limitations and perspectives for DSM.

145 **2. Material and Methods**

146 **2.1. Study area**

147 The study took place within the Peyne river catchment (43.49°N, 3.37°E), located in Southern
148 French Occitanie region (see Figure 1), throughout the year 2015. The spatial extent of the
149 Peyne catchment is around 65 km^2. Altitudes range from 20 to 230 m above sea level. The
150 Peyne catchment is mainly covered by vineyards, mostly rainfed, the remaining being covered
151 by other crops, forests and urban areas. It is typified by a Mediterranean climate, with an annual
152 value of 638 mm and 1109 mm for rainfall and reference evapotranspiration, respectively. The
153 soils depict a large variability in texture and depth, inducing large contrasts in soil moisture
154 regime within the root zone, and thus large contrasts in vine growth conditions (Taylor et al.,
155 2013). Also, permanent or temporary shallow water tables are present in some parts of the
156 catchment, which also affects the availability of water for plants (Guix-Hébrard et al., 2007).

157 **2.2. Site characterizations and ground-based observations**

158 We selected 14 sites (Table 1) which permitted to encompass a large part of the soil variability
159 within the Peyne catchment in terms of SAWC driving factors, namely soil texture, stone con-
160 tent and depth. Ground characterizations at each of the 14 sites were performed (1) to estimate
161 surface soil moisture (SSM) as a constraint variable that could not be obtained from remote

sensing, (2) to determine the observed values of SAWC and of its components that were further compared with model inversions outputs (see § 2.6), and (3) to establish a prior knowledge on soil texture variability used as input of the inversion procedure (see § 2.5.3.1).

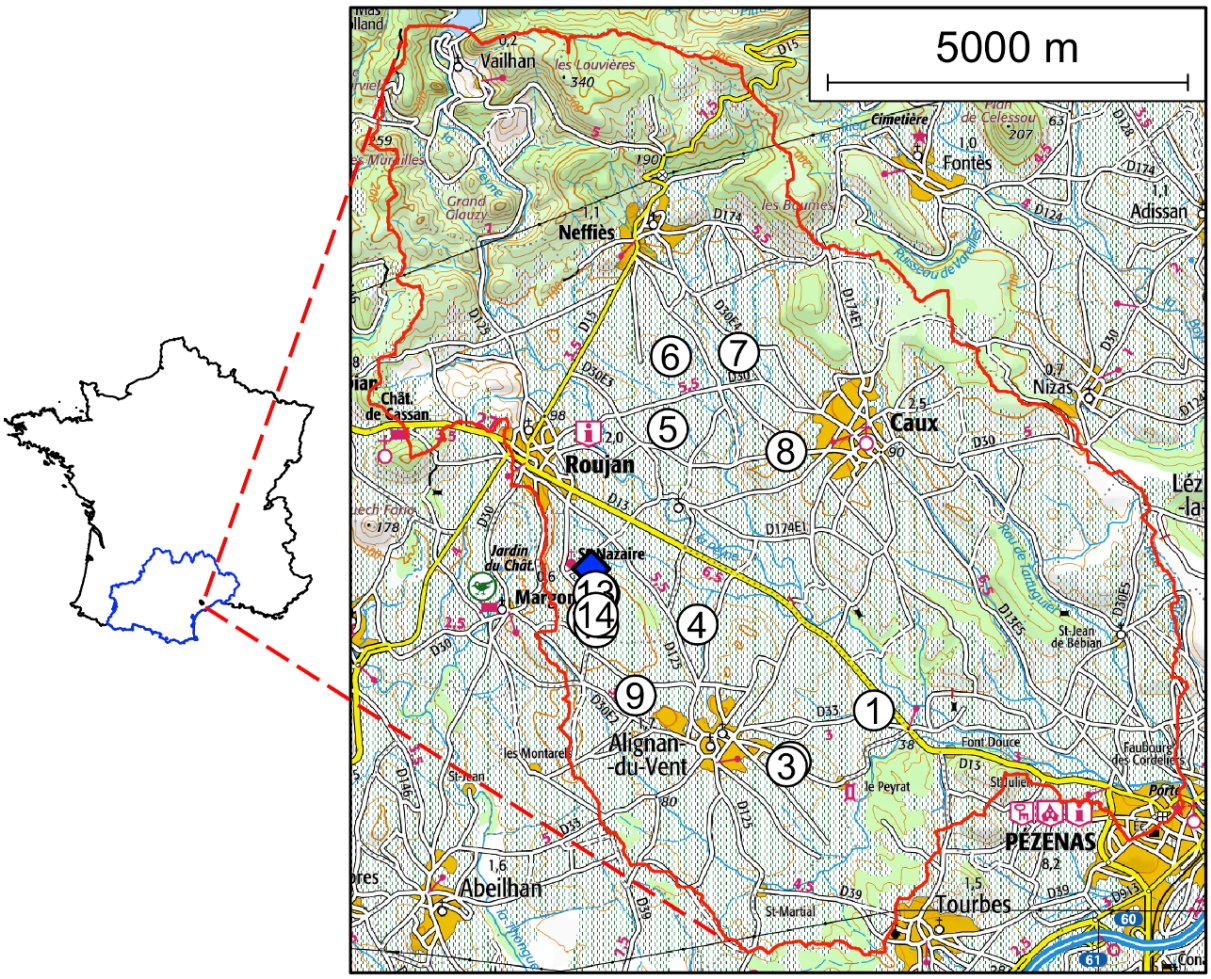

Figure 1. Left: location of the Peyne watershed in the Occitanie region (blue contour). Right: limits of the Peyne watershed (red contour), location of the 14 sites (circles with digits, sites 10-13 are hidden by site 14) and of the Roujan meteorological station (blue diamond).

2.2.1. Soil moisture

Soil moisture profiles were obtained using a 503-DR CPN neutron probe (Vectra, France). Access tubes were set up at 13 sites out of 14. Soil moisture profiles were collected every 15 to 30 days according to rainfall events, between 8 April 2015 and 22 October 2015, which corresponds to 10 dates. Measurements were conducted along the vineyards root zone, from the

subsurface (0.2 - 0.3 m) down to 1.9 m with a 0.2 m step, and from 2.2 m down to 4.2 m with a 0.4 m step. The neutron probe was calibrated against in situ measurements of soil moisture following Galleguillos et al. (2011a; b; 2017). For the remaining site (AW95), hourly soil moisture was recorded using SoilNet sensors (ring oscillators, Bogena et al., 2010), installed at 0.15, 0.3, 0.6, 1.1, 1.5 and 2.0 m depths.

Table 1: description of the sites with ground characterisations. WRB stands for World Reference Base for Soil Resources (https://www.isric.org/explore/wrb).

Site	Name	Geological setting	Soil type (WRB)	soil depth (m)	observed SAWC (mm)
1	Cabrol	Alluvial stony deposits	Fluvisol (skeletic)	2.30	204
2	Peyrat_Bas	Old clayey alluvial deposits	Calcisol (vertic)	2.70	179
3	Peyrat_Haut	Old clayey alluvial deposits	Calcisol (clayic)	1.35	105
4	Cros	Loose sandstone	Gleyic Cambisol	1.55	197
5	Doustheissier	Alluvial stony deposits	Hyperskeletic Cambisol (clayic)	1.20	44
6	Ravanel	Loose sandstone	Calcisol	1.10	155
7	Benoit	Loose sandstone	Leptic Calcisol	1.35	121
8	Panis	Lacustrine limestone	Leptic Calcisol	0.65	123
9	Alary	Lacustrine limestone	Skeletic Calcisol	1.70	129
10	Aw104	Loose sandstone	Calcisol	1.55	202
11	Aw92	Loose sandstone	Calcisol	1.55	202
12	Aw124	Loose sandstone	Calcisol (gleyic)	2.00	208
13	Aw95	Loose sandstone	Calcisol	2.10	185
14	Aw126	Loose sandstone	Calcisol	1.65	217

We used the following procedure for making comparable SoilNet and neutron probe measurements. First, the SoilNet sensors were cross-calibrated with the neutron probe. Second, both neutron probe and SoilNet measurements were normalized along each profile, in accordance to their vertical representativeness. Third, we calculated daily soil moistures from the hourly values. Finally, we used soil moisture records across the [0.2 - 0.3] m layer at all sites to estimate

SSM as a constraint variable of the inversion procedure (see § 2.4). For two sites without direct measurements of SAWC components (aw92 and aw126), the soil moisture records from the subsurface down to 2.4 m were also used as inputs of the SAWC determination procedure (see § 2.2.2).

2.2.2. Ground-based determination of SAWC and its components

On 12 sites out of 14, soil pits were dug or soil cores were drilled in close vicinity of the neutron probe access tubes or of the SoilNet sensors. Soil layers were defined as the soil horizons determined by the morphological observations of the soil profiles, which led to consider between 3 and 5 soil layers. SAWC was classically determined from soil observations and analysis using the following expression (Cousin et al., 2003):

$$SAWC = \sum_{i=1}^{n} D_i * bd_i * \left(\frac{100-st_i}{100}\right) * (HFC_i - HWP_i) \quad (1)$$

where for each soil layer *i,* D_i is the thickness of the layer (mm), bd_i is bulk density, st_i is the coarse fragment content (% volumetric), and HFC_i and HWP_i are the soil moistures at field capacity (FC) and wilting point (WP), respectively. The soil properties bd_i, HFC_i and HWP_i were determined for each layer sample from core sampling using 100 cm^3 stainless-steal cylinders, a pressure plate extractor providing measurements of HFC_i and HWP_i (Klute, 1986). D_i and st_i were determined from the observations made in the soil pits.

For the two remaining sites (aw92 and aw126), we estimated SAWC and its components using the method proposed by Sreelash et al. (2017). The latter consisted of estimating SAWC and its components from a statistical analysis of the times series for soil moisture neutron probe measurements conducted over 10 years at same depths, and at several times each year in accordance to rainfall events. We also applied this method on 5 additional sites, in order to estimate the uncertainty on SAWC components that was required for the inversion approach (see § 2.5.3.1). In order to be consistent with the inversion scheme of the crop model, HFC and

HWP were finally averaged by considering two layers: a topsoil layer (0 - 0.3 m) and a root zone layer (0.3 m to soil depth, derived from observations of D_i made in the soil pits).

2.2.3. Characterization of soil texture variability over the region

Soil samples were collected in 12 sites out of 14, and in three additional sites of the study area, in order to complete the picture of the regional soil variability. Soil samples were collected for each horizon determined by the morphological observations of soil profiles. A total of 77 soil layers (five to six per site) were sampled. The granulometric fractions of the soil samples were determined in the laboratory using classical laboratory techniques (Baize and Jabiol, 1995). The variability of the granulometric fractions as observed on the set of samples is presented in Figure 2.

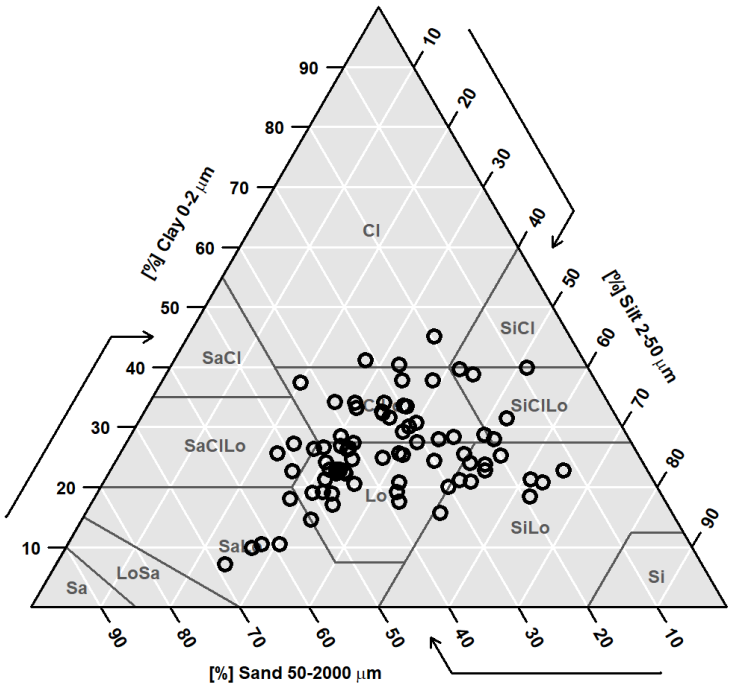

Figure 2: Variability of texture over the 77 soil layers located in the Peyne Catchment.

2.3. Meteorological data

A standard meteorological station (Enerco 400, CIMEL, France) was located in the Roujan head catchment, within the Peyne river catchment (Figure 1). It provided hourly and daily values of solar irradiance, air temperature and humidity, wind speed and rainfall. Reference evapotranspiration ET_0 was calculated following FAO-56 (Allen et al., 1998). Since this meteorological station was installed in 1992 in the framework of the long-term observatory OMERE (Molénat et al., 2018), it allowed the comparison of the hydrological year 2014-2015 (01 September 2014 to 31 August 2015) against the inter-annual average. Hydrological year 2014-2015 was characterized by heavy rainfalls during the fall of 2014 (388 mm), followed by both dry winter (49 mm) and spring (77 mm), and a humid summer (135 mm, that occurred mostly in august, with several high intensity thunderstorms). The cumulated annual rainfall amount was 649 mm, close to the inter-annual average (638 mm). Reference evapotranspiration ET_0 was larger than the inter-annual average, except during august 2015, which led to an annual cumulated ET_0 of 1187 mm, substantially larger than the inter-annual average (1109 mm).

2.4. Constraint variables estimated from satellite images

2.4.1. Landsat 7 ETM+ imagery

Eleven almost cloud-free scenes collected by the Landsat 7 Enhanced Thematic Mapper Plus sensor (ETM+) were available between 8 January 2015 and 23 October 2015. They were downloaded from the U.S. Geological Surveys USGS website, Earth explorer Interface (https://earthexplorer.usgs.gov, accessed June, 01, 2018). These 30-meter resolution images were instrumentally corrected following Vermote et al. (1997), using the calibration factors reported in the downloaded metadata files.

The Landsat images were atmospherically corrected to obtain top of canopy (TOC) reflectances and surface outgoing radiances over the solar (visible and near infrared - NIR) and the thermal infrared (TIR) spectral ranges, respectively. Two atmospheric radiative transfer models were used: the 6S model (Vermote et al., 1997) and the MODTRAN model (Berk et al., 1999) over

248 the solar and TIR spectral range, respectively. The required atmospheric profile data for both
249 models (including pressure, temperature, and relative humidity) were available online
250 (https://atmcorr.gsfc.nasa.gov, accessed on June, 01 2018). There were vertically interpolated
251 using the National Centre for Environmental Prediction (NCEP) reanalysis data (Barsi et al.,
252 2003). Linear interpolation of the aerosol optical thickness (AOT) data at 340, 380, 440, 500,
253 675, 870 and 1020 nm were used to estimate AOT at 550 nm from the Toulouse location
254 (43.562N, 1.476E) of the AERONET network (Holben et al., 2001).

255 Masks were finally created for each acquisition date, to eliminate the missing data caused by
256 the failure of the scan line corrector (SLC) of the Landsat 7 ETM+ sensor (Chen et al., 2010,
257 Li et al., 2017), located in the northwest part of the study area, as well as to eliminate the few
258 clouds and their shadows that occurred for some dates.

259 **2.4.2. Leaf Area Index estimates**

260 In the literature, only few studies were devoted to estimate the leaf area index (LAI) of vine-
261 yards from satellite images. This is due to the discontinuous structure of vineyards canopies
262 (row crops, large bare soil fraction) and to the frequent changes in canopy architecture because
263 of trellis systems and pruning operations. Johnson et al. (2003) showed that LAI of vineyards
264 cultivated in rows can be estimated from normalized difference vegetation index (NDVI) using
265 a linear relationship ($R^2 = 0.72$). Their study covered a wide range of vineyard geometries under
266 Mediterranean climate, and in particular a wide range of row spacings (between 1 and 3.7 me-
267 ters) that included those typically practiced in the Peyne watershed (between 1.8 and 2.5 meter,
268 mainly 2.5). Vineyard LAI maps were thus calculated at 30-meter resolution, using the linear
269 relationship proposed by Johnson et al. (2003):

270 $$LAI = 5.70\ NDVI - 0.25 \qquad (2)$$

271 where NDVI was calculated from ETM+ bands 3 (R: red) and 4 (NIR: near infrared):

$$NDVI = (NIR - R) / (NIR + R) \quad (3)$$

2.4.3. Evapotranspiration estimates

By focusing on the same Peyne watershed, Galleguillos et al. (2011a, 2011b) investigated the mapping of daily ET over vineyards by using the Simplified Surface Energy Balance Index (S-SEBI, Roerink et al., 2000) method, along with ASTER satellite imagery. The latter includes simultaneously observations over the solar (visible and NIR) and the TIR spectral ranges, for the retrieval of albedo and surface temperature, respectively (Jacob et al., 2004; French et al., 2005; 2008). By combining maps of surface albedo and temperature, the S-SEBI model provides estimates of daily ET (Gómez et al., 2005). Thus, Galleguillos et al. (2011a, 2011b) reported an accuracy of 0.8 $mm.day^{-1}$ for the mapping of daily ET over the vineyards of the Peyne watershed, when compared against ground-based references from eddy covariance method. Further, Montes and Jacob (2007) compared the capabilities of ASTER or Landsat 7 ETM+ imageries to retrieve daily ET over the same watershed vineyards, by using the S-SEBI method. They reported a similar accuracy (0.9 $mm.day^{-1}$) when using the Landsat 7 ETM+ imagery, as compared to the use of the ASTER imagery (0.8 $mm.day^{-1}$). For the current study, and on the basis of the above-discussed studies, we followed the approach proposed by Montes and Jacob (2007) for the Landsat 7 ETM + imagery. Thus, we generated daily ET maps with a 30-meter resolution, for each of the 11 Landsat 7 ETM+ imageries collected during the experiment.

2.5. Model inversion approach

Model inversion consists of estimating some model parameters by minimising differences between model simulations and in-situ / remotely sensed measurements (fitting process), for a panel of constraint variables, on the basis of optimization techniques or Bayesian methods (Montes et al., 2014). Obviously, the dynamics of the constraint variables must significantly depend upon the parameters to be estimated, which explains why inversion methods usually involve simultaneous sensitivity studies (Varella et al., 2010b).

297 Several studies were devoted to estimating soil hydrological properties or soil depth, by using
298 different types of models devoted to subsurface water flows (Šimůnek et al., 2016, Galleguillos
299 et al., 2017, Javaux et al., 2008), crop functioning (Florin et al., 2011, Dente et al., 2008 ;
300 Sreelash et al., 2017) or Soil - Vegetation - Atmosphere Transfer (Olioso et al., 2005, Gutmann
301 et al., 2010, Bandara et al., 2015). Follow on from the literature review we discuss in introduc-
302 tion, we considered in the current study the STICS crop model for estimating SAWC compo-
303 nents by inversion, and we selected three constraint variables for the fitting process, either alone
304 or in combination, namely leaf area index (LAI), evapotranspiration (ET) and surface soil mois-
305 ture (SSM). For LAI and ET, we considered the remotely sensed estimates from the Landsat 7
306 ETM+ sensor. For SSM, we considered the in-situ measurements, because remotely sensed
307 estimation of SSM remains questionable over vineyards (Lei et al., 2020).

308 **2.5.1. Implementing the STICS crop model**

309 The STICS crop model (Brisson et al., 1998) was developed to simulate the dynamics of agri-
310 cultural and environmental variables for various crops. STICS is a generic mono-dimensional
311 model (1D vertical fluxes), predicting daily budget of water, carbon and nitrogen within the
312 topsoil and root zone layers, on the basis of energy and mass transfer within the soil - plant -
313 atmosphere continuum. STICS involves more than 200 input parameters or variables, related
314 to soil profile characteristics, plant characteristics according to phenological stages, initialized
315 soil moisture and nitrogen profiles, climate data and agricultural practices (Brisson et al., 1998;
316 2003; Varella et al., 2010a, Guérif et al., 2006). Among many other crops, STICS has been
317 successfully applied to vineyards (Celette and Gary, 2013). In the current study, we used the
318 version V8.41 of the STICS model that can be freely downloaded at the following URL:
319 https://www6.paca.inrae.fr/stics_eng/Download.

320 For the current study, we ran STICS simulations for each of the 14 sites, and we estimated
321 SAWC components from the inversion procedure on the basis of the aforementioned LAI, ET

and SSM estimates. LAI and ET estimates corresponded to the 30-meter pixels of the Landsat 7 ETM+ imagery that matched each of the 14 sites, and SSM estimates corresponded to field measurements within each site (see § 2.2.1). Table 2 summarizes the data used as inputs of STICS simulations to document the model parameters that were not set to default values and the meteorological forcing. The meteorological variables were provided by the Roujan meteorological station (see § 2.2.4). For row geometry of vineyards and other soil parameters that were not estimated for the inversion procedure, we fixed them to single nominal values across the 14 sites, by averaging previous measurements performed within the La Peyne watershed (Meyer, 2016; Molénat et al., 2018). The plant parameters of the wine crop were derived from the STICS library. Soil nitrogen content was set to a standard value for vineyards, also provided by the STICS library. Finally, we used the inversion procedure to fix root zone thickness and hydraulic properties, namely soil moistures at wilting point and field capacity for topsoil and root zone layers (see § 2.5.2). It is worth noting that none of the parameters was obtained by measurements at the site scale, which ensured a potential application of the procedure over the whole watershed.

Table 2: Source of data for documenting the STICS parameters that were not set to the STICS default values and the meteorological forcing. N and C_{org} stand for soil nitrogen content and soil organic carbon, respectively. Vineyard and soil parameters were obtained in the framework of the OMERE environmental observatory (Meyer, 2016; Molénat et al., 2018). The term "scale" stands for the representativeness of the data, either "watershed" for meteorology and for averaged measurements across the 14 sites, or "site" for in-situ data.

	Data	Origin	Scale
Climate	Daily meteorological data	OMERE meteorological station in Roujan	Watershed
Vineyard	Row geometry	Averaged Measurements	Watershed
	Plant functioning parameters	STICS library	Site

Soil	Bulk density	Averaged Measurements	Watershed
	N, C_{org}	Averaged Measurements and STICS Library	Watershed
	Root zone thickness	Estimated from STICS inversion	Site
	Hydraulic properties	Estimated from STICS inversion	Site

The STICS starting simulation date was set to 01 January 2015, after a long period of rainy weather, so that we could initialize soil water content to full water saturation. The ending simulation date was 31 December 2015, thus including the whole cycle of vine cultivation.

2.5.2. Setting up soil layers and soil parameters

In order to reduce the number of STICS parameters to be estimated from inversion, the soil was split into two layers as proposed by Wosten (2001) and Varella (2010b). The boundaries of the topsoil layer (ploughing layer) were set to 0 and 0.3 m depth, and the thickness of the second layer (root zone layer) was included into the set of parameters to be estimated from model inversion. Thus, five soil parameters had to be estimated from the inversion of the STICS model: (1) soil moisture at field capacity HFC_i and wilting point HWP_i for both layers, with i=1 or 2 for the topsoil and root zone layers, respectively, and (2) thickness of root zone layer D_2. The estimated soil available water capacity $SAWC_i$ of each layer was then calculated as:

$$SAWC_i = (HFC_i - HWP_i) \times bd \times D_i \qquad (4)$$

where *bd* is the dry bulk density of layer i, that was set at 1.5 in accordance to the average of dry bulk densities observed in the catchment. Note that the coarse fragment content (sti) in equation 1 is not considered in equation 4, in order to limit the number of soil parameters to be estimated. However, the variations of coarse fragment content were implicitly included into the inversion process through the modulations of the five estimated soil parameters. This point is discussed in § 4.4.

2.5.3. Inversion procedure

For the current study, we used the GLUE method proposed by Beven et al. (1992) to estimate the targeted STICS parameters (root zone thickness as well as soil moistures at wilting point and field capacity for topsoil and root zone layers) along with their uncertainties. This method consists of running the considered model over a large set of model parameter values, referred to as the Numerical Design of Experiment (NDoE) hereafter, by following a given distribution for each parameter. It next selects a subset of parameter values that provide best observation fitting, which leads to the estimates of the parameters along with the associated uncertainties.

The framework we used here was very similar to the classical implementation of the GLUE method, except when generating the population of sampled parameters. Indeed, our framework included two steps: generating the NDoE in a first step, and estimating the parameters and their uncertainties in a second step. Both steps are presented in the next two sections.

2.5.3.1. Generating the Numerical Design of Experiment (NDoE)

The NDoE was the population of SAWC components to be considered as input parameters of the STICS crop model, namely populations of soil moisture at field capacity and wilting point for topsoil layer (HFC_1, HWP_1) and root zone layer (HFC_2, HWP_2), as well as thickness of the root zone layer (D_2). Rather than selecting these SAWC components within independent random distributions, our NDoE aimed to represent the variability of the SAWC components observed within the Peyne watershed. The experiment design was defined according to the following procedure.

- The 77 soil layers sampled in our experiment (see § 2.2.3) were used to define the ranges within which textures were randomly sampled (Table 3). Clay and silt percentages were first randomly selected from uniform distributions bounded by the defined ranges. Sand percentages were then deduced as the complement to 100, and the samples having sand

percentages outside the observed range were eliminated. Given the textures, soil water contents at field capacity (HFC) and at wilting point (HWP) were calculated using the texture-class pedotransfer functions (PTF) proposed by Al Majou et al. (2008, Table 2).

- In order to account for the uncertainties on these values, random noises were next added to HFC and to HWP, following a normal distribution. The standard deviations of the normal distributions were deduced by examining the differences between the SAWC components values determined from the laboratory measurements and those determined from in-situ time series of soil moisture measurements. These differences could be calculated on the 7 sites where both determinations were performed (see § 2.2.2). The standard deviation values were 1.57 and 2.37 for HFC and HWP, respectively.
- We eliminated the samples with HWP values larger than HFC values, to ensure the coherence of the sampled data without SAWC negative values.
- The boundaries of the topsoil layer were set to 0 and 0.3 m depth, according to Wosten et al. (2001) and Varella et al. (2010a). Then, the thickness D_2 of the second layer (root zone layer), was sampled by following a uniform distribution within the prior range adopted by Sreelash et al., (2017) and given in Table 3.

Table 3: Ranges of the parameters used to set up the Numerical Design of Experiment (NDoE).

Parameter	Range	Unit
Clay	7.1 - 45.1	%
Silt	20.0 - 65.2	%
Sand	8.0 - 68.5	%
D_2	0 – 2.7	m

For each location, 20,000 runs of the STICS crop model were conducted, corresponding to each set of the 5 parameters HFC_1, HWP_1, HFC_2, HWP_2 and D_2. All simulated variables of interest were saved in a simulation database for further use.

2.5.3.2. Estimating the parameters

For each of the 14 sites, 11 Landsat 7 ETM+ images were available between January and October 2015, and therefore used to estimate leaf area index (LAI) and daily actual evapotranspiration (ET) (see § 2.4). Additionally, soil moisture measurements in the surface layer (surface soil moisture, SSM) were available on 10 dates between January 2015 and October 2015 (see § 2.2.1). Both Landsat estimates and SSM measurements were used in the inversion process as constraint variables, alone or in combination, which led to six scenarios for estimating SAWC components (Table 4). The first three scenarios involved remotely sensed observations only, whereas the last three scenarios involved both remotely sensed observations and in situ measurements of SSM. On the one hand, we did not consider SSM measurements only in the scenarios because we anticipated that root zone properties (and thus SAWC) could not be retrieved by using SSM only in the inversion system, since SSM corresponds to topsoil moisture. On the other hand, we combined SSM measurements with remotely sensed estimates, in order to quantify the loss of inversion capability when disregarding surface soil moisture as a constraint variable.

Table 4: Scenarios of constraint variables, to be used alone or in combination, for estimating SAWC components by inversion of STICS.

Scenario	**Constraint variables**	**Data source**
L	LAI	Landsat 7 ETM+ imagery
E	ET	
LE	LAI + ET	
LS	LAI + SSM	Landsat 7 ETM+ imagery SSM from field measurements
ES	ET + SSM	
LES	LAI + ET + SSM	

For each run of the STICS model, among the aforementioned 20 000 runs, and each of the six scenarios of constraint variables in Table 4, we computed a likelihood function that compared the STICS simulations against the corresponding observations by combining multiple variables:

426 $$\lambda = \prod_j \left(\sum_k \left[Y_{j,k} - f_{j,k}(P, \theta) \right]^2 \right)^{-(n_j/2+2)} \qquad (5)$$

427 where j specifies the observed variable, k the observation date, $y_{j,k}$ is the observation of the
428 variable j at the date k, $f_{j,k}(P, \theta)$ is the model output of the variable j at the date k, obtained from
429 the model inputs corresponding to the vector of parameters to be estimated θ, P is the vector of
430 STICS parameters whose values are assigned prior to the inversion process, and n_j is the total
431 number of observations of the variable j. The model errors for the different variables are as-
432 sumed to be normally distributed and independent but may have different variances. Starting
433 with the likelihood standard equation that corresponds to these hypotheses, the variance values
434 that maximize this likelihood for fixed θ are substituted to obtain the concentrated likelihood
435 (Seber and Wild, 1989). This allows the combination of information from different response
436 variables, without having to weight them. More details can be found in (Buis et al., 2011) and
437 (Wallach et al., 2011).

438 Then, we selected the 1 000 (5%) parameters vectors HFC_1, HWP_1, HFC_2, HWP_2 and D_2 of the
439 STICS runs having the highest likelihood values λ (equation 5). Finally, each of the five pa-
440 rameters estimates was computed as the mean value of the parameter over the selected set of
441 runs.

442 **2.6. Assessing the reliability of the inversion procedure**

443 Four statistical metrics were considered to assess (1) the goodness-of-fit of the simulations to
444 the observations for the constraint variables, and (2) the goodness-of-fit of the estimated SAWC
445 to their corresponding experimental measurements (see § 2.2.2). These statistical indicators
446 were: Mean Error (ME), Root Mean Square Error (RMSE), Coefficient of determination (R2)
447 and Nash-Sutcliffe model efficiency coefficient (NSE). The definitions of these statistical met-
448 rics are given hereafter:

449 $$ME = \frac{\sum_i^n (P_i - O_i)}{n} \qquad (5)$$

$$RMSE = \sqrt{\frac{\sum_i^n (P_i - O_i)^2}{n}} \quad (6)$$

$$R2 = corr(P_i, O_i)^2 \quad (7)$$

$$NSE = \frac{\sum_1^n (P_i - O_i)^2}{\sum_1^n (O_i - \overline{O})^2} \quad (8)$$

Where P and O stand for predictions and observations, respectively, where observations are the reference for a given variable, and $\bar{O}$ is the averaged value of the observations for a given sample. These statistical metrics were complementary since (1) ME measures the bias between predictions and observations, (2) R^2 measures the strength of the correlation between predictions and observations, independently from the bias, (3) RMSE measures the total error of prediction, including systematic and unsystematic errors, and (4) NSE is an adimensional indicator, related to RMSE, that permits to compare prediction errors across predicted variables and, if positive, to evaluate the percentage of explained variance by the predictions.

It should be noted, however, that in this particular application of the inversion method which consisted in providing soil input for DSM models in a spatially distributed manner, rather than providing local SAWC predictions directly usable for decision making, a special attention was given to R^2. Indeed, the latter accounts for the ability to picture the spatial variability of SAWC across the study region, regardless of bias.

3. Results

3.1. Reproducibility of the constraint variables

We compared the six scenarios of constraint variables for STICS inversion, on their respective goodness-of-fit between (1) observed (SSM) or remotely sensed (LAI and ET) values of the three constraint variables, and (2) simulations of these variables by the inverted STICS model. The results of the comparison are given in Table 5, on the basis of the aforementioned statistical metrics.

Table 5: Statistical metrics for the comparison between (1) observations of the three constraint variables (LAI, ET and SSM), and (2) simulations of these variables by the STICS model after inversion. The comparison is conducted for each of the six inversion scenarios (see Table 4 for definition).

Constraint variable	Scenario	ME	RMSE	R^2	NSE
LAI (m^2/m^2)	L	0.71	1.12	0.32	-1.70
	E	0.62	1.29	0.18	-2.56
	LE	0.67	1.19	0.27	-2.04
	LS	0.75	1.22	0.19	-2.21
	ES	0.64	1.25	0.17	-2.34
	LES	0.71	1.18	0.26	-1.99
ET (mm/day)	L	0.50	1.00	0.38	-0.03
	E	0.40	0.79	0.57	0.34
	LE	0.43	0.83	0.54	0.27
	LS	0.56	1.00	0.38	-0.04
	ES	0.48	0.93	0.44	0.10
	LES	0.47	0.92	0.45	0.11
SSM (g/g)	L	2.61	5.73	0.01	-0.54
	E	1.88	5.12	0.04	-0.22
	LE	1.27	5.44	0.00	-0.38
	LS	0.00	3.38	0.47	0.46
	ES	-0.08	3.40	0.46	0.46
	LES	0.24	3.54	0.42	0.41

The overall quality of prediction of the constraint variables was low with few values of NSE and R^2 exceeding 0.2 and 0.5 respectively (prediction of ET with scenario E and LE, prediction of SSM with scenario LS, ES and LES). However, most of the differences were ascribed to substantial biases (ME) relatively to the total error (RMSE). Also, RMSE values on LAI, ET and SSM were close to the accuracy requirements regularly quoted in literature, namely 0.8 m^2/m^2, 0.8 mm/day and 6.5 %, respectively (Montes & Jacob, 2017, Fang et al., 2019, Prévot et al., 1993). Consequently, the relationships between the observations of the three constraint variables and the simulations of these variables by the inverted STICS model were acceptable. As expected, the smallest differences were obtained on a given constraint variable

when this constraint variable was included into the inverse modelling scenario (L for LAI, E for ET, LS, ES and LES for SSM). Including SSM as a constraint variable (scenarios LS, ES and LES) did not provide significant improvement on LAI and ET estimates. Conversely, it was difficult for STICS to correctly simulate SSM when the latter was excluded from the set of constraint variables (scenarios L, E and LE). Thus, including any constraint variable in the inversion scheme did not lead to better simulations for the other constraint variables (i.e., L versus E and SSM, E versus L and SSM, SSM versus L and E).

3.2. Estimating SAWC components

We compared the six scenarios of constraint variables for STICS inversion, on their respective capabilities to retrieve SAWC components, namely soil parameters HFC_1, HWP_1, HFC_2, HWP_2 and D_2. For that, we compared the retrievals derived from STICS inversion against the ground-based reference derived from the in-situ measurements (see § 2.2.2). The results of the comparison are given in Table 6, on the basis of the aforementioned statistical metrics.

The overall performances of the retrieved SAWC components were low as shown by the negative values of NSE, regardless of SAWC component and scenario (Table 6). Large biases contributed a lot to these low performances, whereas the predicted values were significantly correlated with observed ones (R^2) for some SAWC components and scenarios.

Table 6: comparison of the SAWC components retrieved from STICS inversion against those derived from the in-situ measurements. The SAWC components are soil moisture at field capacity (HFC) and at wilting point (HWP) for topsoil layer (label 1) and root zone layer (label 2), as well as thickness of the root zone layer D_2. The comparison is conducted for each of the six inversion scenarios (see Table 4 for definition).

SAWC component	Scenario	ME	RMSE	R^2	NSE
HFC1	L	-3.28	4.77	0.00	-1.81
(%)	E	-2.76	4.09	0.01	-1.06

	LE	-1.91	3.88	0.03	-0.86
	LS	-0.22	3.12	0.21	-0.20
	ES	-0.12	2.99	0.25	-0.10
	LES	-0.55	2.84	0.28	0.00
HWP1 (%)	L	-1.25	4.32	0.41	-1.08
	E	-0.64	3.29	0.00	-0.20
	LE	0.00	4.12	0.08	-0.89
	LS	1.26	2.60	0.51	0.25
	ES	0.84	2.12	0.60	0.50
	LES	0.70	2.25	0.51	0.44
HFC2 (%)	L	-4.01	5.54	0.01	-1.16
	E	-3.47	5.30	0.00	-0.98
	LE	-3.64	5.64	0.06	-1.24
	LS	-4.70	5.83	0.35	-1.39
	ES	-4.26	5.68	0.01	-1.28
	LES	-4.27	6.00	0.15	-1.53
HWP2 (%)	L	-2.02	3.23	0.00	-0.67
	E	-2.31	3.26	0.15	-0.71
	LE	-2.20	3.23	0.11	-0.67
	LS	-1.61	3.09	0.27	-0.53
	ES	-1.88	3.10	0.03	-0.54
	LES	-1.87	3.20	0.01	-0.64
D_2 (m)	L	0.37	0.63	0.31	-0.55
	E	0.85	0.97	0.15	-2.72
	LE	0.80	0.89	0.41	-2.13
	LS	0.39	0.65	0.05	-0.65
	ES	0.64	0.82	0.02	-1.67
	LES	0.65	0.77	0.35	-1.32

Using all the constraint variables permit to obtain the largest correlation for HFC1 only, and the largest correlations between predictions and observations were obtained with different scenarios, from one SAWC component to another (LES for HFC1, ES for HWP1, LS for HFC2 and HWP2, and LE for D_2). For the topsoil layer, predictions of soil moisture at field capacity (HFC_1) and at wilting point (HWP_1) were best correlated with observations when surface soil moisture (SSM) was included in the set of constraint variables (scenarios LS, ES and LES). For the root zone layer, predictions of soil moisture at field capacity (HFC_2) and at wilting point

515 (HWP_2) were best correlated with observations when LAI and surface soil moisture were in-
516 cluded together in the set of constraint variables (scenario LS). For the thickness of the root
517 zone layer (D2) predictions were best correlated with observations when LAI and ET were used
518 together as constraint variables (scenario LE). Overall, predictions were closer to observations
519 for soil moisture at wilting point as compared to soil moisture at field capacity, apart from the
520 LS scenario for the root zone layer. Also, predictions systematically underestimated (respec-
521 tively overestimated) observations for HFC (respectively D_2), whereas predictions systemati-
522 cally underestimated observations for HWP in root zone layer only (possible overestimation for
523 HWP in topsoil layer).

524 **3.3. Estimating SAWC**

525 We compared the six scenarios of constraint variables for STICS inversion, on their respective
526 capabilities to retrieve SAWC, calculated from the estimated SAWC components as defined in
527 Equation 4. For that, we compared the retrievals derived from STICS inversion against the
528 ground-based reference derived from the in-situ measurements (see § 2.2.2). The results of the
529 comparison are given in Table 7, on the basis of the aforementioned statistical metrics.

530 The RMSE on SAWC estimated from the STICS inversion were larger than 60 mm with nega-
531 tive values of NSE and small R^2 values, which denoted poor predictions. Biases (ME) were
532 large, especially for the scenario E and LE, and often positive, which indicated a global over-
533 estimation of SAWC.

534 *Table 7: comparison of the SAWC retrievals from STICS inversion against those derived from*
535 *the in-situ measurements. The comparison is conducted for each of the six inversion scenarios*
536 *(see Table 4 for definition).*

Scenarios	ME (mm)	RMSE (mm)	R2	NSE
L	10.89	70.51	0.15	-1.07
E	71.11	113.86	0.01	-4.39

LE	59.57	98.43	0.01	-3.03
LS	-21.51	51.60	0.14	-0.11
ES	17.50	67.11	0.05	-0.87
LES	18.86	64.42	0.04	-0.73

To explain these overall poor performances, a critical analysis of each of the 14 sites was conducted, which led to distinguish three sites with peculiar soil water conditions:

- The "Peyrat-Haut" and "Doustheissier" showed clear evidences of additional water supply for vineyard, namely (1) lateral flows caused by recurrent overflows from a nearby ditch for the "Peyrat-Haut" site (Site #3 on Figure 1), and (2) the presence of a shallow watertable fed by the Peyne river for the "Doustheissier" site (Site #5 on Figure 1).
- The "Cabrol" site (Site #1 on Figure 1) was characterized by a soil profile with hydromorphic characteristics for the deep soil layers revealing the occurrence of temporary waterlogging (Tassinari et al., 2002).

Removing these three sites induced significant increases of performances for the LE scenario (ME = 52 mm, RMSE = 70 mm, NSE = -3.08 and R^2 = 0.47) and, more importantly, for the LES scenario (ME = 9 mm RMSE = 31 mm, NSE = 0.17 and R^2 = 0.58). Figures 3a and 3b display the scatterplots when comparing the individual SAWC predictions against the corresponding reference observations for these two scenarios, showing the three sites with peculiar soil water conditions. Finally, these gains of performance when removing the three aforementioned sites were mainly due to significant increases in the prediction performances for root zone thickness (R^2 = 0.68 for scenario LE, R^2 = 0.58 for scenario LES).

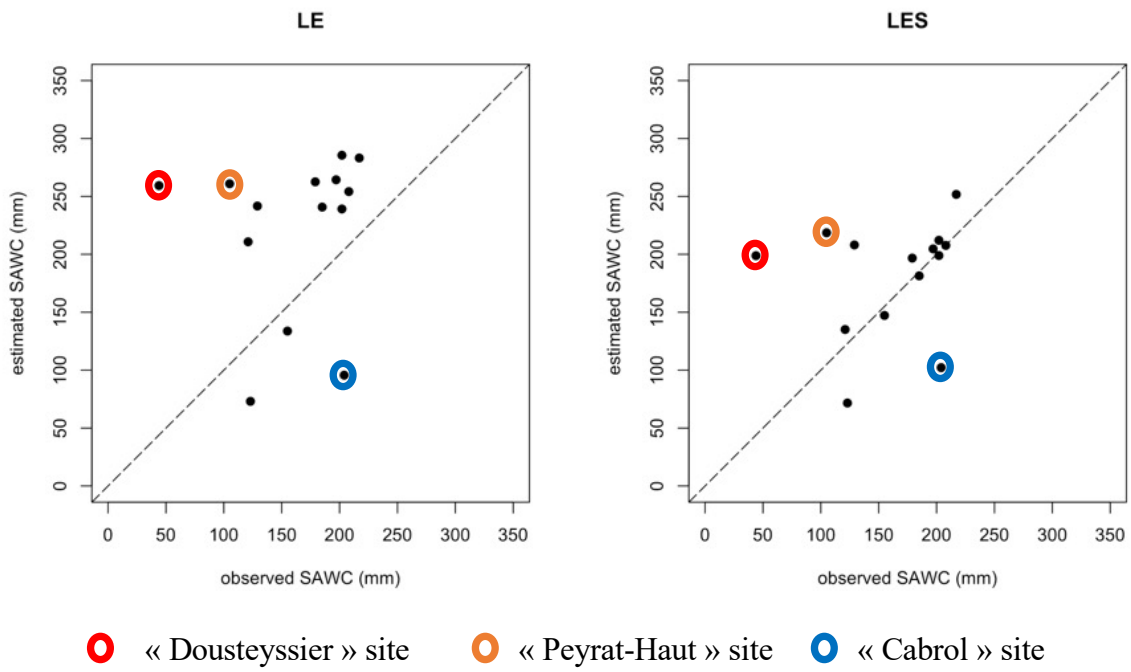

554

555 *Figure 3: Predicted vs observed SAWC for scenario LE (LAI and ET as constraint variables)*
556 *and LES (LAI, ET and SSM as constraint variables)*

557 **4. Discussion**

558 **4.1. Overall performances of SAWC predictions**

559 To the best of our knowledge, this study is the first that evaluated a crop model inversion ap-
560 proach for predicting SAWC and its components in the current operational conditions of Digital
561 Soil Mapping, namely over a large spatial extent with landscape heterogeneities, by considering
562 discontinuous crops, and by including a large panel of plant status indicators derived from sat-
563 ellite imagery. The results we obtained revealed poor prediction performances both for SAWC
564 and its components. However, the best prediction performances we obtained for SAWC as a
565 whole with the LES scenario, after the removal of sites with peculiar soil water conditions, were
566 comparable with those reported in the few field-scale studies dedicated to the estimation of
567 SAWC from crop model inversion. Indeed, Morgan et al. (2003) and Jiang et al. (2008) reported
568 RMSEs respectively between 37 to 74 mm and 18 to 50 mm, respectively. Such performances

569 were also comparable to those obtained over the same study area at a different period by Cou-
570 louma et al. (2020) when predicting SAWC from carbon isotope discrimination ($\delta^{13}C$) in har-
571 vested grapes (RMSE between 35 and 61 mm). Besides, substantial parts of the prediction er-
572 rors were due to biases (as measured by ME), whereas some scenarios showed significant cor-
573 relations between predictions and ground measurements, with R^2 values up to 0.6. Finally, us-
574 ing SSM as constraint variable in addition to LAI and/or ET led to better predictions of SAWC.

575 Better results could theoretically be obtained by determining site specific values of STICS pa-
576 rameters (e.g., bulk density, row geometry of wine crops, soil nitrogen content etc…) instead
577 of setting constant values for these parameters across the whole study area. Some of these pa-
578 rameters (e.g., raw spacing) can be spatialized using remote sensing techniques (Delenne et al,
579 2010). However, most of the STICS parameters cannot be locally determined in the absence of
580 any available proxy (e.g., soil nitrogen content), which makes unrealistic their spatialisation at
581 large scale because of subsequent errors that are difficult to reduce. Additionally, the spatial
582 mismatching between soil measurements (soil profile over 1 m × 1 m) and remotely sensed
583 constraint variables (pixels over 30 m × 30 m) can generate errors that may affect the inversion
584 procedure. Indeed, variographic studies performed in the same region showed that a non-neg-
585 ligible part of the soil property variations occurred at very short scale (Gomez et al, 2012, Fig-
586 ure 3). Finally, it can be anticipated that several nonreducible factors such as those cited above
587 may limit the precision of SAWC estimations. A sensitivity analysis of the inversion procedure
588 is necessary to study the respective impacts of these factors, and to identify the site specific
589 properties to be characterized first for further improvements.

590 **4.2. Comparisons of performances across scenario and SAWC components**

591 This study compared several scenarios involving different constraint variables among which
592 evapotranspiration (ET) that, contrary to leaf area index (LAI) and surface soil moisture SSM,
593 has been rarely considered in the literature.

On the one hand, errors on simulations and / or observations of constraint variables (LAI, ET, SSM) were decorrelated from one variable to another. On the other hand, the sensitivities of constraint variables to the soil properties obtained from STICS inversion changed from one variable to another. This explained why (1) including any constraint variable in the inversion scheme did not lead to better simulations for the other constraint variables, (2) the best prediction performances for soil properties were not obtained with a unique set of constraint variables, and (3) combining together the three constraint variables did not systematically provide the best prediction performances for SAWC and components, apart from the prediction of SAWC as a whole after removal of the three sites with peculiar soil water conditions.

The prediction performances obtained for the SAWC components with different scenarios of constraint variables were physically consistent with our knowledge of the underlying physical processes. First, we obtained better performances for soil moisture at field capacity and wilting point in the soil surface layer when including surface soil moisture (SSM) into the set of constraint variables. Second, we obtained better retrieving performances for soil moisture at wilting point than for soil moisture at field capacity. This was ascribed to large occurrences of water stress periods with soil moisture close to wilting point throughout the vine growth cycle, as compared to low occurrences of water availability periods with soil moisture close to field capacity. These large / low occurrences could also explain why predictions systematically underestimated observations for soil moisture at field capacity. Third, it was necessary combining ET and LAI as constraint variables to obtain significant correlations between predictions and observations for (1) SAWC components within the root zone layer and (2) SAWC as a whole after the removal of the three sites with peculiar soil water conditions. This was explained by the strong dependence of vegetation transpiration and growth upon root zone SAWC and components, especially when vegetation faced water shortages.

Including ET as a constraint variable permitted to increase the prediction of soil properties related to the root zone layer, which underlines the importance of developing robust methods to estimate ET from remote sensing, where current challenges are related to discontinuous canopies, heterogeneous landscapes and hilly areas (Aouade et al., 2020; Bellvert et al., 2021; Boudhina et al., 2018; Merlin et al., 2014; Zitouna et al., 2012; 2015; 2018). Similarly, including SSM as a constraint variable permitted to increase the prediction of soil moisture at field capacity and wilting point in the soil surface layer, which motivates continued efforts on the retrieval of surface soil moisture from remote sensing (Babaeian et al., 2019; Paolini et al., 2021), and especially over complex crop canopies such as vineyard (Fernandez-Moran et al., 2015).

4.3. Study area peculiarities, strengths and limitations

This study addressed the retrieving of SAWC from crop model inversion within a Mediterranean vineyard. The specificities of the study area should be thoroughly analysed to better understand our results and to anticipate possible improvements or applications to other areas.

Following Sreelash et al. (2017), the retrieval quality of SAWC components from model inversion depends upon the agro-pedo-climatic conditions of the study area. Indeed, the latter drive the modelling capabilities to account for vegetation types within the study area, while the performances of the inversion largely depend upon the modelling capabilities to reproduce the link between vegetation functioning and water uptakes within deep soil layers.

- In that respect, rainfed vineyard catchments can be considered as favourable areas for crop model inversion. Vineyards are the dominant crops in such areas, which makes the crop model inversion applicable on numerous sites covering a large variety of soils. Also, grape vine is rarely irrigated, which makes the crop sensitive to deep soil characteristics and water content, thus facilitating the crop model inversion. Todoroff et al. (2010) observed that rainfed sugar cane in dry years was another example of favourable agro-climatic conditions for predicting SAWC from crop model inversion.

- Also, cropping systems with large water dynamics that include wetting and drying cycles should be optimal for estimating SAWC components from crop model inversion (Sreelash et al., 2017). This is not completely the case for the study reported in the current paper, with larger occurrence of drying periods, which lead to large biases for the prediction of root zone soil moisture at field capacity (§ 4.2).
- Finally, the specific climate conditions observed during the period of experiment increased the limitations of our SAWC predicting approach from crop model inversion. In the example of scenarios LE and LES shown in Figure 3, SAWC was strongly underestimated at two sites ("Peyrat-Haut" and "Doustheissier") because of allochthonous water supplies from shallow watertable or nearby ditches (see § 3.3) during summer 2015 thunderstorms. Besides, Figure 3 revealed that SAWC predictions strongly underestimated observations at the "Cabrol" site with morphological evidence of temporary waterlogging. Such temporary waterlogging was likely to occur during the experiment period after the wet autumn 2014 (358 mm), with subsequent depletions of the rooting systems that hampered the full exploitation of the available water within the root zone layers. In such site-specific conditions, the crop model could not represent water flows correctly, and the subsequent errors propagated into the SAWC predictions. Besides, these errors might have been amplified by the well-known spatial heterogeneities of the rainfalls in this Mediterranean area (Ducrocq et al., 2014), that were not considered in our approach.

From this analysis, it can be deduced that SAWC prediction from crop model inversion could be largely improved in the future by moving to a multi-annual approach. This would permit to increase the number of wetting and drying cycles and to select the years with climatic conditions that attenuate the site-specific problems discussed above. As an example, by adopting such a multi-annual approach (four years) and by selecting years with favourable climate conditions (three years out of four), Coulouma et al. (2020) increased their SAWC prediction performances

from carbon isotope discrimination ($\delta^{13}C$) in the harvested grapes, with RMSE decreasing from [35 - 61] mm to 32 mm. Besides, rainfall heterogeneities could be better addressed in the future by replacing climatic records from a unique weather station with high resolution rain maps as now provided by terrestrial radar systems (Lengfeld et al., 2020).

4.4. SAWC concept mismatches

It should be noted that the SAWC field measurements (see § 2.2.2) and predictions from crop model inversion (see § 2.5) did not share the same underlying concepts. On the one hand, the SAWC field measurements relied on a "soil-based" approach involving static soil parameters that together represent the maximum soil water storage to sustain plant transpiration, as stated by Cousin et al. (submitted). On the other hand, the crop model inversion was a "plant-based approach" involving proxies of water quantity withdrawn from soil by vegetation throughout the crop growth cycle. Our study is a good illustration of statement by Cousin et al. (submitted): "Depending on the climate conditions, this AWC-equivalent parameter [provided by the plant-based approach] can be strongly different from the AWC evaluated from soil-based approaches. In some situations, it can even be close to the Readily Available Water Content".

Additionally, the SAWC field measurements (see § 2.2.2) and predictions from crop model inversion (see § 2.5) did not rely on the same description of soil properties. On the one hand, the SAWC field measurements relied on dug soil pits and drilled soil cores to characterize profiles of soil properties across different layers, with consideration for coarse fragment content. On the other hand, the crop model inversion procedure considered two layers only, namely topsoil and root zone layers, without explicitly consideration for coarse fragment content, although profiles of soil properties and coarse fragment content were implicitly included into the inversion procedure, since they drove plant status indicators to be used as constraint variables (LAI, ET, SSM).

In spite of these differences in both underlying concepts and description of soil properties, we observed that the crop model inversion provided useful predictions of "soil-based" SAWC in most of the sites (11 sites out of 14 in black on figure 3). This demonstrated that both approaches can be combined to better map SAWC over regional extents, in spite of their different underlying concepts and description of soil properties. Again, a critical analysis of the overall climate and topography, as well as of the soil specific conditions, should permit to avoid large errors caused by these differences.

4.5 Implications for Digital Soil Mapping

We explored a potential way to estimate SAWC in a spatially distributed manner, as this property is sorely lacking in current databases. This new approach complements other means previously explored such as $\delta^{13}C$ (Coulouma et al., 2020). As it does not require direct numerous field measurements, it is quite inexpensive and open path for having a high spatial density of characterised sites.

Lagacherie and Gomez (2018) mentioned two ways of using remotely sensed data for DSM: either as exhaustive covariates, or as a provider of point sites characterised by the property to be mapped. In view of the results, which clearly show the impossibility of obtaining an exhaustive estimate of the SAWC due to particular situations that model inversion cannot consider, the prospects for using SAWC estimates by model inversion clearly lie in the second way. The introduction of these new data can therefore be considered as "soft data" in co-kriging procedures, as already done with hyperspectral data (Walker et al., 2017) and with Field EM38 measurements (Zare et al., 2021). It should be noted that such approaches require only that the "soft data" should be well-correlated with the target soil property, and are unsensitive to large biases as those observed in our results.

To fully achieve the hybridization of model inversion techniques and Digital Soil Mapping, data flow from the latter to the former should also be considered. In this study, the numeric

717 design of experiment of the inversion procedure used ranges of SAWC-related soil properties
718 (Table 3) that were deduced from the existing laboratory samples in the study area. Alternate
719 determinations of these ranges could also be deduced from excerpts of prior DSM products
720 available at the national or regional scales (Chen et al., 2022) and covering the study area.

721 **5. Conclusion**

722 The main lessons that can be retrieved from this study are the following.

723 • Using crop model inversion with remotely sensed variables related to vegetation transpira-
724 tion (ET), vegetation growth (LAI) and surface soil moisture (SSM) could potentially allow
725 the estimation of Soil Available Water Capacity and its components at low cost (no ground
726 soil measurements) and over large areas.

727 • The comparisons against ground measurements of SAWC in a Mediterranean vineyard re-
728 vealed overall poor estimation performances. However, acceptable correlations with ground
729 measurements of SAWC (R2 = 0.47 and 0.58) were obtained for specific scenarios of con-
730 straint variables (LAI + ET, LAI + ET + SSM) after the removal of specific sites with pe-
731 culiar soil-water conditions. Surface Soil moisture was also found potentially useful for
732 predicting surface soil hydrodynamic properties.

733 • The poor estimation performances stemmed from a minority of sites for which unmodelled
734 processes (allochthonous water supply, waterlogging) occurred under the particular condi-
735 tions during the experiment period (wet autumn).

736 • With a multi-annual approach increasing the number of wetting and drying cycles, while
737 avoiding site-specific unmodelled processes, crop model inversion approach could be used
738 in the future for providing spatial sampling of SAWC and of its components, to be next
739 used as surrogate input data for Digital Soil Mapping models.

740 **6. Acknowledgements.**

This study was conducted in the framework of the RUEdesSOLS project, financed by the French National Research Agency, through grants ANR-14-CE01-0011-01, ANR-14-CE01-0011-02, ANR-14-CE01-0011-04 and ANR-14-CE01-0011-08. The authors thank Nicolas Meyer, Anna Nassibe, Jean-Luc Belotti and David Fages for their significant contribution in collecting the field data used for this study.

7. References

Adhikari, K., Hartemink, A.E., 2016. Linking soils to ecosystem services - A global review. Geoderma 262, 101–111.

Allen, R. G., Pereira, L. S., Raes, D., & Smith, M. (1998). Crop evapotranspiration-Guidelines for computing crop water requirements-FAO Irrigation and drainage paper 56. FAO, Rome, 300(9), D05109.

Al Majou, H., Bruand, A., Duval, O., Le Bas, C. Vautier, A., 2008. Prediction of soil water retention properties after stratification by combining texture, bulk density and the type of horizon. Soil Use and Management, 24(4): 383-391.

Aouade, G., Jarlan, L., Ezzahar, J., Er-Raki, S., Napoly, A., Benkaddour, A., Khabba, S., Boulet, G., Garrigues, S., Chehbouni, A. Boone, A., 2020. Evapotranspiration partition using the multiple energy balance version of the ISBA-Ag s land surface model over two irrigated crops in a semi-arid Mediterranean region (Marrakech, Morocco). Hydrology and Earth System Sciences, 24(7), 3789-3814.

Babaeian, E., Sadeghi, M., Jones, S. B., Montzka, C., Vereecken, H., & Tuller, M., 2019. Ground, proximal, and satellite remote sensing of soil moisture. Reviews of Geophysics, 57(2), 530-616.

Baize D., Jabiol B., 1995. Guide pour la description des sols. INRA ed, 375 p.

764 Bandara, R., Walker, J. P., Rüdiger, C., & Merlin, O., 2015. Towards soil property retrieval
765 from space: An application with disaggregated satellite observations. Journal of Hydrology,
766 522, 582-593.
767 Barsi, J.A., Barker, J.L., Schott, J.R., 2003. An atmospheric Correction Parameter Calculator
768 for a Single Thermal Band Earth-Sensing Instrument. In Proceedings of the 2003 IEEE In-
769 ternational Geoscience and Remote Sensing Symposium (IEEE Cat. No.03CH37477), Tou-
770 louse, France, 21–25 July 2003; 3014–3016.
771 Bellvert, J., Nieto, H., Pelechá, A., Jofre-Čekalović, C., Zazurca, L., & Miarnau, X., 2021. Re-
772 mote sensing energy balance model for the assessment of crop evapotranspiration and water
773 status in an almond rootstock collection. Frontiers in Plant Science, 12, 288.
774 Berk, A., Anderson, G.P., Bernstein, L.S., Acharya, P.K., Dothe, H., Matthew, M.W., Adler-
775 Golden, S.M., Chetwynd, J.H., Richtsmeier, S.C., Pukall, B., Allred, C.L., Jeong, L.S.,
776 Hoke, M.L. 1999. MODTRAN4 radiative transfer modelling for atmospheric correction.
777 Proceedings of SPIE Optical Spectroscopic Techniques and Instrumentation for Atmos-
778 pheric and Space Research III, 3756, 1999. Bellingham WA 98227-0010 USA.
779 Beven, K. J., A. M. Binley. The future of distributed models: Model calibration and uncertainty
780 prediction, Hydrological Processes, 1992, 6, 279–298.
781 Bogena, H. R., Herbst, M., Huisman, J. A., Rosenbaum, U., Weuthen, A., & Vereecken, H.,
782 2010. Potential of wireless sensor networks for measuring soil water content variability. Va-
783 dose Zone Journal, 9(4), 1002-1013.
784 Boudhina, N., Zitouna-Chebbi, R., Mekki, I., Jacob, F., Ben Mechlia, N., Masmoudi, M., &
785 Prévot, L., 2018. Evaluating four gap-filling methods for eddy covariance measurements of
786 evapotranspiration over hilly crop fields. Geoscientific Instrumentation, Methods and Data
787 Systems, 7(2), 151-167.

788 Brisson, N., Mary, B., Ripoche, D., Hélène, M., Ruget, F., Nicoullaud, B., Gate, P., Devienne-
789 Barret, F., Recous, S., C, X.T., Plenet, D., Cellier, P., Machet, J., Marc, J., Delécolle, R.,
790 1998. STICS : a generic model for the simulation of crops and their water and nitrogen bal-
791 ances. 1. Theory and parameterization applied to wheat and corn 18, 311–346.
792 Brisson, N., Gary, C., Justes, E., Roche, R., Mary, B., Ripoche, D., Zimmer, D., Sierra, J.,
793 Bertuzzi, P., Burger, P., Bussière, F., Cabidoche, Y.M., Cellier, P., Debaeke, P., Gaudillère,
794 J.P., Maraux, F., Seguin, B., Sinoquet, H., 2003. An overview of the crop model STICS.
795 European Journal of Agronomy, 18, 309-332.
796 Buis, S., Wallach, D., Guillaume, S., Varella, H., Lecharpentier, P., Launay, M., Guerif, M.,
797 Bergez, J.E., Justes, E., 2011. The STICS crop model and associated software for analysis,
798 parameterization and evaluation. In: Ahuja L.R. and Ma L. (Eds.), "Methods of Introducing
799 System Models into Agricultural Research". Advances in Agricultural Systems Modeling 2.
800 American Society of Agronomy, Crop Science Society of America, and Soil Science Society
801 of America, Madison, 395-426.
802 Celette, F., Gary, C., 2013. Dynamics of water and nitrogen stress along the grapevine cycle as
803 affected by cover cropping. European Journal of Agronomy 45, 142–152.
804 Charoenhirunyingyos, S., Honda, K., Kamthonkiat, D., Ines, A.V.M., 2011. Soil hydraulic pa-
805 rameters estimated from satellite information through data assimilation. International Jour-
806 nal of Remote Sensing 32, 8033–8051.
807 Chen, F., L. Tang, Qiu, Q., 2010. Exploitation of CBERS-02B as Auxiliary Data in Recovering
808 the Landsat7 ETM+ SLC-Off Image, 18th IEEE International Conference on Geoinformat-
809 ics, 2010, 1–6.
810 Chen, S., Arrouays, D., Leatitia, V., Poggio, L., Minasny, B., Roudier, P., Libohova, Z.,
811 Lagacherie, P., Shi, Z., Hannam, J., Meersmans, J., Richer-de-forges, A.C., Walter, C.,

2022. Digital mapping of GlobalSoilMap soil properties at a broad scale : A review. Geoderma 409, 115567.

Coops, N.C., Waring, R.H. Hilker, T., 2012. Prediction of soil properties using a process-based forest growth model to match satellite-derived estimates of leaf area index. Remote Sensing of Environment, 126: 160-173.

Coudert, B., Ottlé, C., Boudevillain, B., Demarty, J., Guillevic, P., 2006. Contribution of Thermal Infrared Remote Sensing Data in Multiobjective Calibration of a Dual-Source SVAT Model. Journal of Hydrometeorology, 7(3), 404-420

Coulouma, G., Prévot, L., & Lagacherie, P., 2020. Carbon isotope discrimination as a surrogate for soil available water capacity in rainfed areas: A study in the Languedoc vineyard plain. Geoderma, 362, 114121.

Cousin, I., Nicoullaud, B., & Coutadeur, C., 2003. Influence of rock fragments on the water retention and water percolation in a calcareous soil. Catena, 53(2), 97-114.

Cousin, I., Buis, S., Lagacherie, P., Doussan, C., Le Bas, C., Guérif, M., submitted. The Available Water Capacity, from a multidisciplinary and multiscale standpoint. A review. Agriculture for Sustainable Development.

Dejong, R., Shields, J.A., 1988. Available Water-holding capacity maps of Alberta, Saskatchewan and Manitoba. Canadian Journal of Soil Science, 68(1): 157-163.

Delenne, C., Durrieu, S., Rabatel, G., Deshayes, M., 2010. From pixel to vine parcel: A complete methodology for vineyard delineation and characterization using remote-sensing data. Computers and Electronics in Agriculture, 70, 78-83.

Dente, L., Satalino, G., Mattia, F., Rinaldi, M., 2008. Assimilation of leaf area index derived from ASAR and MERIS data into CERES-Wheat model to map wheat yield. Remote Sens. Environ. 112, 1395–1407.

836 Dong, J., Steele-Dunne, S.C., Ochsner, T., Hatch, C.E., Sayde, C., Selker, J., Tyler, S., Cosh,
837 M.H., van de Giesen, N., 2016. Mapping high-resolution soil moisture and properties using
838 distributed temperature sensing data and an adaptive particle batch smoother. Water Re-
839 sources Research, 52(10), 7690-7710.
840 Ducrocq, V., Braud, I., Davolio, S., Ferretti, R., Flamant, C., Jansa, A., Kalthoff, N., Richard,
841 E., Taupier-Letage, I., Ayral, P., Belamari, S., Berne, A., Borga, M., Boudevillain, B., Bock,
842 O., Boichard, J., Bouin, M., Bousquet, O., Bouvier, C., Chiggiato, J., Cimini, D., Corsmeier,
843 U., Coppola, L., Cocquerez, P., Defer, E., Delanoë, J., Di Girolamo, P., Doerenbecher, A.,
844 Drobinski, P., Dufournet, Y., Fourrié, N., Gourley, J. J., Labatut, L., Lambert, D., Le Coz,
845 J., Marzano, F. S., Molinié, G., Montani, A., Nord, G., Nuret, M., Ramage, K., Rison, W.,
846 Roussot, O., Said, F., Schwarzenboeck, A., Testor, P., Van Baelen, J., Vincendon, B., Aran,
847 M., & Tamayo, J., 2014. HyMeX-SOP1: The Field Campaign Dedicated to Heavy Precipi-
848 tation and Flash Flooding in the Northwestern Mediterranean, Bulletin of the American Me-
849 teorological Society, 95(7), 1083-1100.
850 Eisele, A., Chabrillat, S., Hecker, C., Hewson, R., Lau, I.C., Rogass, C., Segl, K., Cudahy, T.J.,
851 Udelhoven, T., Hostert, P., Kaufmann, H., 2015. Advantages using the thermal infrared
852 (TIR) to detect and quantify semi-arid soil properties. Remote Sens. Environ. 163, 296–311.
853 Fang, H., Baret, F., Plummer, S., & Schaepman-Strub, G., 2019. An overview of global leaf
854 area index (LAI): Methods, products, validation, and applications. Reviews of Geophysics,
855 57, 739-799.
856 Feddes, R. A., Menenti, M., Kabat, P., & Bastiaanssen, W. G. M., 1993. Is large-scale inverse
857 modelling of unsaturated flow with areal average evaporation and surface soil moisture as
858 estimated from remote sensing feasible? Journal of hydrology, 143(1-2), 125-152.
859 Fernandez-Moran, R., Wigneron, J.-P., Lopez-Baeza, E., Al-Yaari, A., Coll-Pajaron, A., Mi-
860 alon, A., Miernecki, M., Parrens, M., Salgado-Hernanz, P.M., Schwank, M., Wang, S., Kerr,

Y.H., 2015. Roughness and vegetation parameterizations at L-band for soil moisture retrievals over a vineyard field. Remote Sensing of Environment, Volume 170, 269-279.

Ferrant, S., Bustillo, V., Burel, E., Salmon-Monviola, J., Claverie, M., Jarosz, N., Yin, T., Rivalland, V., Dedieu, G., Demarez, V., Ceschia, E., Probst, A., Al-Bitar, A., Kerr, Y., Probst, J.L., Durand, P., Gascoin, S., 2016. Extracting soil water holding capacity parameters of a distributed agro-hydrological model from high resolution optical satellite observations series. Remote Sensing, 8(2): 154.

Florin, M. J., McBratney, A. B., Whelan, B. M., & Minasny, B., 2011. Inverse meta-modelling to estimate soil available water capacity at high spatial resolution across a farm. Precision Agriculture, 12(3), 421-438.

French, A.N., Jacob, F., Anderson, M.C., Kustas, W.P., Timmermans, W., Gieske, A., Su, Z., Su, H., McCabe, M.F., Li, F., Prueger, J., Brunsell, N., 2005. Surface energy fluxes with the Advanced Spaceborne Thermal Emission and Reflection radiometer (ASTER) at the Iowa 2002 SMACEX site (USA). Remote Sens. Environ. 99, 55–65.

French, A. N., Schmugge, T. J., Ritchie, J. C., Hsu, A., Jacob, F., & Ogawa, K. E. N. T. A., 2008. Detecting land cover change at the Jornada Experimental Range, New Mexico with ASTER emissivities. Remote Sensing of Environment, 112(4), 1730-1748.

Galleguillos, M., Jacob, F., Prévot, L., Lagacherie, P., Liang, S., 2011a. Mapping daily evapotranspiration over a Mediterranean vineyard watershed. IEEE Geoscience and Remote Sensing Letters, 8(1), 168-172.

Galleguillos, M., Jacob, F., Prévot, L., French, A., Lagacherie, P., 2011b. Comparison of two temperature differencing methods to estimate daily evapotranspiration over a Mediterranean vineyard watershed from ASTER data. Remote Sens. Environ. 115.

884 Galleguillos, M., Jacob, F., Prévot, L., Faúndez, C., Bsaibes, A., 2017. Estimation of actual
885 evapotranspiration over a rainfed vineyard using a 1-D water transfer model: A case study
886 within a Mediterranean watershed. Agricultural Water Management 184, 67–76.
887 Gómez, M., Olioso, A., Sobrino, J. A., & Jacob, F., 2005. Retrieval of evapotranspiration over
888 the Alpilles/ReSeDA experimental site using airborne POLDER sensor and a thermal cam-
889 era. Remote Sensing of Environment, 96(3-4), 399-408.
890 Gomez, C., Lagacherie, P., Coulouma, G., 2012. Regional predictions of eight common soil
891 properties and their spatial structures from hyperspectral Vis-NIR data. Geoderma 189–190.
892 Guerif, M., Houlès, V., Makowski, D., Lauvernet, C., 2006. Data assimilation and parameter
893 estimation for precision agriculture using the crop model STICS. In: Wallach, D., Makow-
894 ski, D., Jones, J.W. (Eds.), Working with Dynamic Crop Models. Elsevier, 395–401.
895 Guillevic, P.C., Privette, J.L., Coudert, B., Palecki, M.A., Demarty, J., Ottlé, C., Augustine,
896 J.A., 2012. Land Surface Temperature product validation using NOAA's surface climate
897 observation networks—Scaling methodology for the Visible Infrared Imager Radiometer
898 Suite (VIIRS). Remote Sens. Environ. 124, 282–298.
899 Guix-Hébrard, N., Voltz, M., Trambouze, W., Garnier, F., Gaudillère, J.P., Lagacherie, P.,
900 2007. Influence of watertable depths on the variation of grapevine water status at the land-
901 scape scale. European Journal of Agronomy 27.
902 Gutmann, E. D., & Small, E. E., 2010. A method for the determination of the hydraulic prop-
903 erties of soil from MODIS surface temperature for use in land-surface models. Water Re-
904 sources Research, 46(6).
905 Holben, B.N., Tanre, D., Smirnov, A. Eck, T.F., Slutsker, I., Abuhassan, N., Newcomb, W.W.,
906 Schafer, J.S., Chatenet, B., Lavenu, Kaufman, Y.J., Vande Castle, J., Setzer, B., Markham,
907 D., Clark, R., Frouin, R., Halthore, A., Karneli, N.T.O., Neill, C., Pietras, R.T., Pinker, K.,

908 Zibordi Voss, G. 2001. An emerging ground-based climatology: Aerosol optical depth from
909 AERONET. Journal of Geophysical Research, 106 (D11), 12067-12097.
910 Jacob, F., Petitcolin, F., Schmugge, T., Vermote, É., French, A., Ogawa, K., 2004. Comparison
911 of land surface emissivity and radiometric temperature derived from MODIS and ASTER
912 sensors. Remote Sens. Environ. 90, 137–152.
913 Javaux, M., Schröder, T., Vanderborght, J., & Vereecken, H., 2008. Use of a three-dimensional
914 detailed modelling approach for predicting root water uptake. Vadose Zone Journal, 7(3),
915 1079-1088.
916 Jiang, P., Kitchen, N. R., Anderson, S. H., Sadler, E. J., & Sudduth, K. A., 2008. Estimating
917 plant-available water using the simple inverse yield model for claypan landscapes. Agron-
918 omy Journal, 100(3), 830-836.
919 Jin, X.X., Wang, S., Yu, N., Zou, H.T., An, J., Zhang, Y.L., Wang, J.K., Zhang, Y.L., 2018a.
920 Spatial predictions of the permanent wilting point in arid and semi-arid regions of Northeast
921 China. Journal of Hydrology, 564: 367-375.
922 Jin, X., Kumar, L., Li, Z., Feng, H., Xu, X., Yang, G., Wang, J., 2018b. A review of data as-
923 similation of remote sensing and crop models. European Journal of Agronomy 92, 141–152.
924 Jhorar, R. K., Van Dam, J. C., Bastiaanssen, W. G. M., & Feddes, R. A., 2004. Calibration of
925 effective soil hydraulic parameters of heterogeneous soil profiles. Journal of Hydrology,
926 285(1-4), 233-247.
927 Johnson, L.F., Roczen, D.E., Youkhana, S.K., Nemani, R.R., Bosch, D.F., 2003. Mapping vine-
928 yard leaf area with multispectral satellite imagery. Computer @ Electronic in Agriculture.
929 38: 33-44
930 Klute, A., 1986. Water retention: Laboratory methods. In: Klute, A., (Ed.), Methods of Soil
931 Analysis, Part 1-Physical and Mineralogical Methods, 2nd Edition. Agronomy Monograph
932 9. American Society of Agronomy-Soil Science Society of America,

933 Knighton, J., Singh, K., Evaristo, J., 2019. Understanding Catchment - Scale Forest Root Water
934 Uptake Strategies Across the Continental United States Through Inverse Ecohydrological
935 Modeling. Geophysical Research Letter 47, e2019GL085937.
936 Kool, D., Ben-Gal, A., Agam, N., Šimůnek, J., Heitman, J. L., Sauer, T. J., & Lazarovitch, N.,
937 2014. Spatial and diurnal below canopy evaporation in a desert vineyard: Measurements and
938 modelling. Water Resources Research, 50(8), 7035-7049.
939 Lagacherie, P., Gomez, C., 2018. Vis-NIR-SWIR Remote Sensing Products as New Soil Data
940 for Digital Soil Mapping, in: McBratney, A.B., Minasny, B., Stockman, U., (Eds.), Pedomet-
941 rics. Springer.
942 Lagouarde, J.-P., Bach, M., Sobrino, J.A., Boulet, G., Briottet, X., Cherchali, S., Coudert, B.,
943 Dadou, I., Dedieu, G., Gamet, P., Hagolle, O., Jacob, F., Nerry, F., Olioso, A., Ottlé, C.,
944 Roujean, J., Fargant, G., 2013. The MISTIGRI thermal infrared project: scientific objectives
945 and mission specifications. International Journal of Remote Sensing 34, 3437–3466.
946 Lammoglia, S. K., Chanzy, A., & Guerif, M., 2019. Characterizing soil hydraulic properties
947 from Sentinel 2 and STICS crop model. In 2019 IEEE International Workshop on Metrology
948 for Agriculture and Forestry (MetroAgriFor), 312-316.
949 Launay, M., Guerif, M., 2005. Assimilating remote sensing data into a crop model to improve
950 predictive performance for spatial applications. Agriculture Ecosystem Environment, 111,
951 321–339.
952 Leenhardt, D., Voltz, M., Bornand, M., Webster, R., 1994. Evaluating soil maps for prediction
953 of soil-water properties. European Journal of Soil Science, 45(3): 293-301.
954 Leenaars, J.G.B., Claessens, L., Heuvelink, G.B.M., Hengl, T., Ruiperez González, M., van
955 Bussel, L.G.J., Guilpart, N., Yang, H., Cassman, K.G., 2018. Mapping rootable depth and
956 root zone plant-available water holding capacity of the soil of sub-Saharan Africa. Geoderma
957 324, 18–36.

Lei, F., Crow, W.T., Kustas, W.P., Dong, J., Yang, Y., Knipper, K.R., Anderson, M.C., Gao, F., Notarnicola, C., Greifeneder, F., McKee, L.M., Alfieri, J.G., Hain, C., Dokoozlian, N., 2020. Data assimilation of high-resolution thermal and radar remote sensing retrievals for soil moisture monitoring in a drip-irrigated vineyard. Remote Sens. Environ. 239, 111622.

Lengfeld, K., Kirstetter, P., Fowler, H.J., Yu, J., Becker, A., 2020. Use of radar data for characterizing extreme precipitation at fine scales and short durations Use of radar data for characterizing extreme precipitation at fine scales and short durations. Environ. Res. Lett. 15, 085003.

Li, C., Zheng, Y; Wu, Y., 2017. Recovering missing pixels for Landsat ETM + SLC- off imagery using HJ-1A /1B as auxiliary data, International Journal of Remote Sensing, 38:11, 3430-444.

Merlin, O., Chirouze, J., Olioso, A., Jarlan, L., Chehbouni, G., & Boulet, G., 2014. An image-based four-source surface energy balance model to estimate crop evapotranspiration from solar reflectance/thermal emission data (SEB-4S). Agricultural and Forest Meteorology, 184, 188-203.

Mertens, J., Madsen, H., Feyen, L., Jacques, D., & Feyen, J., 2004. Including prior information in the estimation of effective soil parameters in unsaturated zone modelling. Journal of Hydrology, 294(4), 251-269.

McBratney, A.B., Mendonca-Santos, M.D., Minasny, B., 2003. On digital soil mapping. Geoderma 117, 3–52.

McBratney, A.B., Field, D.J., Koch, A., 2014. Geoderma The dimensions of soil security. Geoderma 213, 203–213.

Meyer, N., 2016. Suivi de l'eau disponible pour la vigne : évaluation du modèle STICS en contexte languedocien. MSc. Dissertation in Water Sciences, University of Montpellier.

Molénat J., Raclot, D., Zitouna, R., Andrieux, P., Coulouma, G., Feurer, D., Grünberger, O., Lamachère, J.M., Bailly, J.S., Belotti, J.L., K., B.A., Ben Mechlia, N., Ben Younès Louati, M., Biarnès, A., Blanca, Y., Carrière, D., Chaabane, H., Dagès, C., Debabria, A., Dubreuil, A., Fabre, J.C., Fages, D., Floure, C., Garnier, F., Geniez, C., Gomez, C., Hamdi, R., Huttel, O., Jacob, F., Jenhaoui, Z., Lagacherie, P., Le Bissonnais, Y., Louati, R., Louchart, X., Mekki, I., Moussa, R., Negro, S., Pépin, Y., Prévot, L., Samouelian, A., Seidel, J.L., Trotoux, G., Troiano, S., Vinatier F., Zante, P., Zrelli, J., Albergel, J., Voltz, M., 2018. OMERE: A Long-Term Observatory of Soil and Water Resources, in Interaction with Agricultural and Land Management in Mediterranean Hilly Catchments. Vadose Zone Journal 17.

Montes, C., Lhomme, J. P., Demarty, J., Prévot, L., & Jacob, F., 2014. A three-source SVAT modelling of evaporation: Application to the seasonal dynamics of a grassed vineyard. Agricultural and forest meteorology, 191, 64-80.

Montes C., Jacob, F. 2017. Comparing Landsat-7 ETM+ and ASTER Imageries to Estimate Daily Evapotranspiration Within a Mediterranean Vineyard Watershed, IEEE Geoscience and Remote Sensing Letters, 14(3), 459-463.

Montzka, C., Moradkhani, H., Weihermüller, L., Franssen, H.H., Canty, M., Vereecken, H., 2011. Hydraulic parameter estimation by remotely-sensed top soil moisture observations with the particle filter. Journal of Hydrology 399, 410–421.

Morgan, C. L., Norman, J. M., & Lowery, B., 2003. Estimating plant-available water across a field with an inverse yield model. Soil Science Society of America Journal, 67(2), 620-629.

Olioso, A., Braud, I ; Chanzy, A ; Courault, D., Demarty, J., Kergoat, L., Lewan, E., Ottlée, C., Prévot, L., Zhao, W.G., Calvet, J.C., Cayrol, P., Jongschaap, R., Moulin, S., Noilhan, J., Wigneron, J.P. 2002. SVAT modelling over the Alpilles-ReSeDA experiment: comparing SVAT models over wheat fields. Agronomie 22, 651–668.

Olioso, A., Inoue, Y., Ortega-Farias, S., Demarty, J., Wigneron, J. P., Braud, I., Jacob, F., Lecharpentier, P., Ottlé, C., Calvet, J.-C., Brisson, N., 2005. Future directions for advanced evapotranspiration modelling: Assimilation of remote sensing data into crop simulation models and SVAT models. Irrigation and Drainage Systems, 19(3), 377-412.

Paolini, G., Escorihuela, M. J., Bellvert, J., & Merlin, O., 2021. Disaggregation of SMAP Soil Moisture at 20 m Resolution: Validation and Sub-Field Scale Analysis. Remote Sensing, 14(1), 167.

Piedallu, C., Gégout, J. C., Bruand, A., & Seynave, I., 2011. Mapping soil water holding capacity over large areas to predict potential production of forest stands. Geoderma, 160(3-4), 355-366.

Prévot, L., Champion, I; Guyot, G., 1993. Estimating Surface Soil-Moisture and Leaf-Area Index of a Wheat Canopy Using a Dual-Frequency (C And X-Bands) Scatterometer, Remote Sensing of Environment, 46(3), 331-339, DEC 1993.

Prévot, L., Chauki, H., Troufleau, D., Weiss, M., Baret, F., Brisson, N., 2003. Assimilating optical and radar data into the STICS crop model for wheat. Agronomy 23.

Ridler, M.E., Sandholt, I., Butts, M., Lerer, S., Mougin, E., Timouk, F., Kergoat, L., Madsen, H., 2012. Calibrating a soil–vegetation–atmosphere transfer model with remote sensing estimates of surface temperature and soil surface moisture in a semi-arid environment. Journal of Hydrology 436–437, 1–12.

Roerink, G. J., Su, Z., & Menenti, M., 2000. S-SEBI: a simple remote sensing algorithm to estimate the surface energy balance. Physics and Chemistry of the Earth. Part B: Hydrology, Oceans and Atmosphere, 25(2), 147−157.

Roman Dobarco, M., Bourennane, H., Arrouays, D., Saby, N.P.A., Cousin, I., Martin, M.P., 2019. Uncertainty assessment of GlobalSoilMap soil available water capacity products : A French case study. Geoderma 344, 14–30.

1031 Scharnagl, B., Vrugt, J., Vereecken, H., Herbst, M., 2011. Inverse modelling of in situ soil
1032 water dynamics: Investigating the effect of different prior distributions of the soil hydraulic
1033 parameters. Hydrology and Earth System Sciences, 15(10): 3043-3059.
1034 Seber, G.A.F., Wild, C.J., 1989. Nonlinear Regression. Wiley, New York.
1035 Šimůnek, J., Van Genuchten, M. T., & Šejna, M., 2016. Recent developments and applications
1036 of the HYDRUS computer software packages. Vadose Zone Journal, 15(7), vzj2016-04.
1037 Singh, U. K., Ren, L., & Kang, S., 2010. Simulation of soil water in space and time using an
1038 agro-hydrological model and remote sensing techniques. Agricultural Water Management,
1039 97(8), 1210-1220.
1040 Sreelash, K., Buis, S; Sekhar, M., Ruiz, L., Tomer, S.K., Guérif. M., 2017. Estimation of avail-
1041 able water capacity components of two-layered soils using crop model inversion: effect of
1042 crop type and water regime. Journal of Hydrology, 546, 166-178
1043 Styc, Q., Lagacherie, P., 2021. Uncertainty assessment of soil available water capacity using
1044 error propagation : A test in Languedoc-Roussillon. Geoderma 391, 114968.
1045 Tassinari, C., Lagacherie, P., Bouzigues, R., Legros, J. P., 2002. Estimating soil water satura-
1046 tion from morphological soil indicators in a pedologically contrasted Mediterranean region.
1047 Geoderma, 108, 225-235.
1048 Taylor, J.A., Jacob, F., Galleguillos, M., Prévot, L., Guix, N., Lagacherie, P., 2013. The utility
1049 of remotely-sensed vegetative and terrain covariates at different spatial resolutions in mod-
1050 elling soil and watertable depth (for digital soil mapping). Geoderma 193–194.
1051 Todoroff, P., De Robillard, F., & Laurent, J. B., 2010. Interconnection of a crop growth model
1052 with remote sensing data to estimate the total available water capacity of soils. In 2010 IEEE
1053 International Geoscience and Remote Sensing Symposium (1641-1644). IEEE.
1054 USDA-NCRS, 2008. Soil quality indicators. https://www.nrcs.usda.gov/Internet/FSE_DOCU-
1055 MENTS/nrcs142p2_053288.pdf (accessed on December 2nd 2021)

1056 Van Looy, K., Bouma, J., Herbst, M., Koestler, J., Minasny, B., Mishra, U., Montzka, C.,
1057 Nemes, A., Pachepsky, Y., Padarian, J., Schaap, M.G., Tóth, B., Verhoef, A., Vanderborght,
1058 J., van der Ploeg, M.J., Weihermüller, L., Zacharias, S., Zhang, Y., Vereecken, H. 2017.
1059 Pedotransfer functions in Earth system science: Challenges and perspectives. Reviews of
1060 Geophysics, 55, 1199-1256.
1061 Varella, H., Guerif, M., Buis, S., Beaudoin, N., 2010a. Soil properties estimation by inversion
1062 of a crop model and observations on crops improves the prediction of agro-environmental
1063 variables. European Journal of Agronomy, 33(2): 139-147.
1064 Varella, H., Guérif, M., & Buis, S., 2010b. Global sensitivity analysis measures the quality of
1065 parameter estimation: The case of soil parameters and a crop model. Environmental Model-
1066 ling & Software, 25(3), 310-319.
1067 Vaudour, E., Gomez, C., Fouad, Y., Lagacherie, P., 2019. Sentinel-2 image capacities to predict
1068 common topsoil properties of temperate and Mediterranean agroecosystems. Remote Sens.
1069 Environ. 223, 21–33.
1070 Veihmeyer, F.J., Hendrickson, A.H., 1927. Soil moisture condition in relation to plant growth.
1071 Plant Physiology, 2: 72-81.
1072 Vermote, E.F., Tanre, D., Deuze, J.L., Herman, M., Morcette, J.J., 1997. Second simulation of
1073 the satellite signal in the solar spectrum, 6S: An overview. IEEE Transactions on Geoscience
1074 and Remote Sensing, 35(3), 675–686. Walker, E., Monestiez, P., Gomez, C., Lagacherie, P.,
1075 2017. Combining measured sites, soilscapes map and soil sensing for mapping soil proper-
1076 ties of a region. Geoderma 300.
1077 Wallach, D., Buis, S., Lecharpentier, P., Bourges, J., Clastre, P., Launay, M., Bergez, J.-E.,
1078 Guerif, M., Soudais, J., Justes, E., 2011. A package of parameter estimation methods and
1079 implementation for the STICS crop-soil model. Environmental Modelling & Software,
1080 26(4), 386-394,

Wilford, J., 2006. The Use of Airborne Gamma-ray Imagery for Mapping Soils and Understanding Landscape Processes, in: Lagacherie, P., McBratney, A.B., Voltz, M. (Eds.), Digital Soil Mapping: An Introductory Perspective. Springer, 207–218.

Wosten, J. H. M., Pachepsky, Y. A., Rawls, W. J., 2001. Pedotransfer functions: bridging the gap between available basic soil data and missing soil hydraulic characteristics. Journal of Hydrology, 251: 123-150.

Zare, S., Abtahi, A., Rashid, S., Shamsi, F., Lagacherie, P., 2021. Combining laboratory measurements and proximal soil sensing data in digital soil mapping approaches. Catena 207, 105702.

Zitouna-Chebbi, R., Prévot, L., Jacob, F., Mougou, R., & Voltz, M., 2012. Assessing the consistency of eddy covariance measurements under conditions of sloping topography within a hilly agricultural catchment. Agricultural and Forest Meteorology, 164, 123-135.

Zitouna-Chebbi, R., Prévot, L., Jacob, F., & Voltz, M., 2015. Accounting for vegetation height and wind direction to correct eddy covariance measurements of energy fluxes over hilly crop fields. Journal of Geophysical Research: Atmospheres, 120(10), 4920-4936.

Zitouna-Chebbi, R., Prévot, L., Chakhar, A., Marniche-Ben Abdallah, M., & Jacob, F., 2018. Observing actual evapotranspiration from flux tower eddy covariance measurements within a hilly watershed: Case study of the Kamech site, Cap Bon Peninsula, Tunisia. Atmosphere, 9(2), 68.